Molecular Cancer Research

Heparanase Promotes Glioma Progression and Is Inversely Correlated with Patient Survival

Soumi Kundu[1], Anqi Xiong[1], Argyris Spyrou[1], Grzegorz Wicher[1], Voichita D. Marinescu[2], Per-Henrik D. Edqvist[1], Lei Zhang[1], Magnus Essand[1], Anna Dimberg[1], Anja Smits[3], Neta Ilan[4], Israel Vlodavsky[4], Jin-Ping Li[2], and Karin Forsberg-Nilsson[1]

Abstract

Malignant glioma continues to be fatal, despite improved insight into its underlying molecular mechanisms. The most malignant form, glioblastoma (GBM), is characterized by aberrant activation of receptor tyrosine kinases (RTK) and infiltrative growth. Heparan sulfate proteoglycans (HSPG), integral components of the extracellular matrix of brain tumors, can regulate activation of many RTK pathways. This prompted us to investigate heparanase (HPSE), which cleaves HSPGs, for its role in glioma. This hypothesis was evaluated using tissue microarrays, GBM cells derived from patients, murine *in vitro* and *in vivo* models of glioma, and public databases. Downregulation of HPSE attenuated glioma cell proliferation, whereas addition of HPSE stimulated growth and activated ERK and AKT signaling. Using HPSE transgenic and knockout mice, it was demonstrated that tumor development *in vivo* was positively correlated to HPSE levels in the brain. HPSE also modified the tumor microenvironment, influencing reactive astrocytes, microglia/monocytes, and tumor angiogenesis. Furthermore, inhibition of HPSE reduces tumor cell numbers, both *in vitro* and *in vivo*. HPSE was highly expressed in human glioma and GBM cell lines, compared with normal brain tissue. Indeed, a correlation was observed between high levels of HPSE and shorter survival of patients with high-grade glioma. In conclusion, these data provide proof-of-concept for anti-HPSE treatment of malignant glioma, as well as novel insights for the development of HPSE as a therapeutic target.

Implications: This study aims to target both the malignant brain tumor cells per se and their microenvironment by changing the level of an enzyme, HPSE, that breaks down modified sugar chains on cell surfaces and in the extracellular space. *Mol Cancer Res; 14(12); 1243–53. ©2016 AACR.*

Introduction

Gliomas are the most common form of brain tumors, and if of high grade, gliomas almost always lead to poor outcome, in particular glioblastoma (GBM). Despite surgery, followed by combined radiotherapy and chemotherapy, the median survival for GBM patients is 15 months (1). Molecular subgrouping of GBM by expression profiling and large-scale characterization of genetic alterations (2) has highlighted the extreme heterogeneity of this disease. Unfortunately, to date, research in this area has helped prolong patient survival only marginally (1). In addition to its rapid proliferation and extensive heterogeneity, GBM is highly invasive (3, 4). Indeed, one of its hallmarks is diffuse infiltration of neoplastic cells into healthy brain tissue. The tumor microenvironment contains several infiltrating cell types that support tumor growth (5), and a better understanding of the interaction between cancer cells and their milieu could provide novel therapeutic strategies (6, 7), which motivates detailed investigation of the extracellular matrix (ECM) associated with glioma.

Heparan sulfate proteoglycans (HSPGs) are major constituents of this ECM (8). They contain a core protein to which repeating disaccharide units have been added. The specific structures of HS are achieved through a number of enzymatic steps that create highly charged, sulfated microdomains (9, 10). The resulting HSPGs influence biological processes by interacting specifically with a large number of different physiologically important molecules. In addition, HSPGs can sequester growth factors and thereby modulate their bioavailability in the microenvironment. Heparanase (HPSE), an endo-glucuronidase, is the major enzyme of degradation in this context, cleaving the HS side-chains of HSPGs to release fragmented HS (11). Upregulation of this enzyme in several human cancers is associated with more extensive tumor metastasis and reduced postoperative survival (12–16).

Our hypothesis that HPSE also regulates progression of glioma was evaluated here using murine glioma, patient-derived GBM, tissue microarrays (TMA), and public databases. We provide evidence that HPSE enhances the proliferation and viability of glioma cells by influencing ERK and AKT signaling. HPSE levels in the mouse brain affected glioma growth and influenced the tumor microenvironment. Elevated expression of HPSE was found to be associated with shorter patient survival and, furthermore, an

[1]Department of Immunology, Genetics and Pathology, Science for Life Laboratory, Uppsala University, Uppsala, Sweden. [2]Department of Medical Biochemistry and Microbiology, Science for Life Laboratory, Uppsala University, Uppsala, Sweden. [3]Department of Neuroscience, Neurology, Uppsala University, Uppsala, Sweden. [4]Cancer and Vascular Biology Research Center, The Ruth and Bruce Rappaport Faculty of Medicine, Technion, Haifa, Israel.

Note: Supplementary data for this article are available at Molecular Cancer Research Online (http://mcr.aacrjournals.org/).

Corrected online March 9, 2018

Corresponding Author: Karin Forsberg-Nilsson, Uppsala University, Dag Hammarskjolds vag 20, 751 85 Uppsala, Sweden. Phone: +46184714158; Fax: +46184712000; E-mail: karin.nilsson@igp.uu.se

doi: 10.1158/1541-7786.MCR-16-0223

inhibitor of HPSE effectively reduced glioma growth, indicating that this enzyme may be a valuable multifunctional therapeutic target in GBM.

Materials and Methods

Cell culture

The mouse GL261 glioma cell line was a kind gift from Dr. G. Safrany, NRIRR, and was cultured as described (17). The human GBM cell cultures (U30XXMG) are part of the Uppsala University Human Glioma Cell Culture (HGCC) bio bank and were cultured as described (18). CHO-HPSE and CHO-V_0 cells were cultured as described (19). HGCC cell lines were verified by short tandem repeat profiling (18), whereas GL261 and CHO cells were not authenticated, but all cell lines were screened for mycoplasma using the MycoAlert PLUS Mycoplasma Detection Kit (Lonza).

Immunofluorescence and immunohistochemistry staining

Cells were grown on polyornithine-and laminin-coated coverslips. Immunoflourescence staining was performed as described in (20) using the primary antibody Ab733 (19) diluted 1:200. The secondary antibody was goat anti-rabbit Alexa 488 (Life Technologies). For staining of F-actin filaments, cells were incubated with a 1:1,000 dilution of Alexa flour 568 Phalloidin (Life Technologies) for 1 hour at room temperature.

Tissue sections (5 μm) of paraffin-embedded mouse brains were prepared as described (20). Primary antibodies: rabbit anti-heparanase 733 (19), mouse anti-GFAP (Sigma-Aldrich), rat anti-mouse CD31 (Dianova), rabbit anti-mouse Desmin (Abcam), and rat anti-mouse Mac2 (Cedarlane Laboratories Ltd). Secondary antibodies: donkey anti-rat Cy3 (Fisher Scientific), donkey anti-mouse (Jackson ImmunoResearch), and goat anti-rabbit Alexa 488 (Life Technologies).

Monitoring proliferation and viability

Conditioned medium was collected and filtered 24 hours after addition of DMEM without serum to CHO-HPSE and CHO-V_0 cells, and added 1:1 with fresh medium to serum-starved GL261 cells. Viable cells were quantified by trypan blue exclusion using a Countess Cell Counter (Life Technologies).

For live cell counting, GL261 cells were serum-starved for 18 hours, and thereafter serum-containing medium with additives (rHPSE or PG545, Progen; diluted in PBS) was added. The cells were analyzed in a live-content IncuCyte imaging system (Essen Biosciences).

GL261 cells were cultured in serum-containing medium overnight and Alamar blue added (vol:vol ratio 1:10). The absorbance at 530/560 was measured in a Perkin Elmer Wallac Victor microplate reader (PerkinElmer).

Western blotting

Cells were lyzed in ice-cold RIPA buffer (http://www.abcam.com/protocols/buffer-and-stock-solutions-for-western-blot#RIPA) containing 1 mmol/L of phenylmethylsulfonylfluoride, 0.5% Pefablock, 1% sodium orthovanadate, and 1% protease inhibitor cocktail (Roche). Equal amounts of protein were loaded onto lanes for 10% NuPAGE (Life Technologies) and thereafter were transferred using iBlot gel transfer nitrocellulose stacks (Life Technologies). The membranes were blotted as described in ref. 21. The following primary antibodies were used: rabbit polyclonal anti-heparanase 733 (19), rabbit polyclonal anti-p44/42 MAPK (Erk1/2), anti–phoshpo-p44/42 MAPK (Erk1/2; Thr202/Tyr204), anti–phospho-Akt (Ser473), and anti-Akt (all from Cell Signaling) and anti–beta-actin from (Sigma-Aldrich). The secondary antibodies were horseradish peroxidase–conjugated anti-mouse or anti-rabbit IgG (GE Healthcare).

Lentivirus transduction

For targeted downregulation of HPSE in human GBM, the nucleotide sequence ^{423}GGAATCAACCTTTGAAGAG^{441} was employed (22). The double-stranded nucleotide was cloned into a pBMN vector controlled by the H1 promoter and GFP expression driven by the CMV promoter (pBMN-sh HPSE: CMV-GFP-luc-H1-sh HPSE, pBMN-NTS: CMV-GFP-luc-H1-sh NTS). For monitor GL261 cell *in vivo*, the lentiviral vector pBMN (GFP-Luc) was used for transduction. Lentiviral particle production has been described (23). Lentivirus mixed with polybrene (7.5 μg/mL; Sigma-Aldrich) was added to the cells (70% confluent), and 24 hours later, cells were transferred to medium with puromycin (1.5 μg/mL; Sigma-Aldrich).

qPCR

For specific amplification of the HPSE gene, the forward primer was: CGGCTAAGATGCTGAAGAGC and the reverse primer: TGATGCCATGTAACTGAATCAA. RNA extraction and qPCR were performed as described (20). Data are represented as RQ values, normalized to the Ct value (for endogenous β-actin), and calculated relative to the experimental control.

Quantification of immunofluorescent staining of tissue sections

Stained sections were visualized with the Zeiss Axio Imager 2 (Carl Zeiss), and images captured using the same exposure time in the acquisition mode of ZEN2 blue 2012 software (Carl Zeiss). Stained images were quantitated using the Image J software (imagej.nih.gov/ij/).

Mouse strains

C57Bl/6J mice (6–8 weeks old) were from Taconic M&B. The HPSE knockout (Hpse-KO) and transgenic (Hpse-Tg) mice on C57Bl/6J background have been described previously (24, 25). All mouse experiments were performed in accordance with Swedish legislation, and approved by the local Ethics Committee for Laboratory Animals.

Treatment of GL261-induced subcutaneous tumors with the HPSE inhibitor

Gl261/GFP/Luc cells (3×10^6) in a volume of 100 μL were injected into the flank of mice. Tumors size was measured using a Vernier caliper and tumor volume then calculated from the formula length $\times$ (width)^2 $\times$ 0.5. The HPSE inhibitor PG545 (Progen) was then administered at a dose of 20 mg/kg/week, and tumors measured three times every week. Mice were sacrificed when tumors reached a volume of 1 cm^3.

Intracranial glioma and bioluminescence imaging

One microliter of Gl261/GFP/Luc cells (10^4 cells/μL) were then injected stereotactically 1 mm anterior to bregma, 1.5 mm from the mid-line, and 2.75 mm below the cranial surface using a 10-μL Hamilton syringe. Thereafter, the mice were monitored for signs of tumors (hunched posture, lethargy, or weight loss >10%) daily for 3 weeks and sacrificed when such symptoms appeared. For histologic evaluation, the mice were anesthetized and perfused transcardially with 1$\times$ PBS and 4% paraformaldehyde.

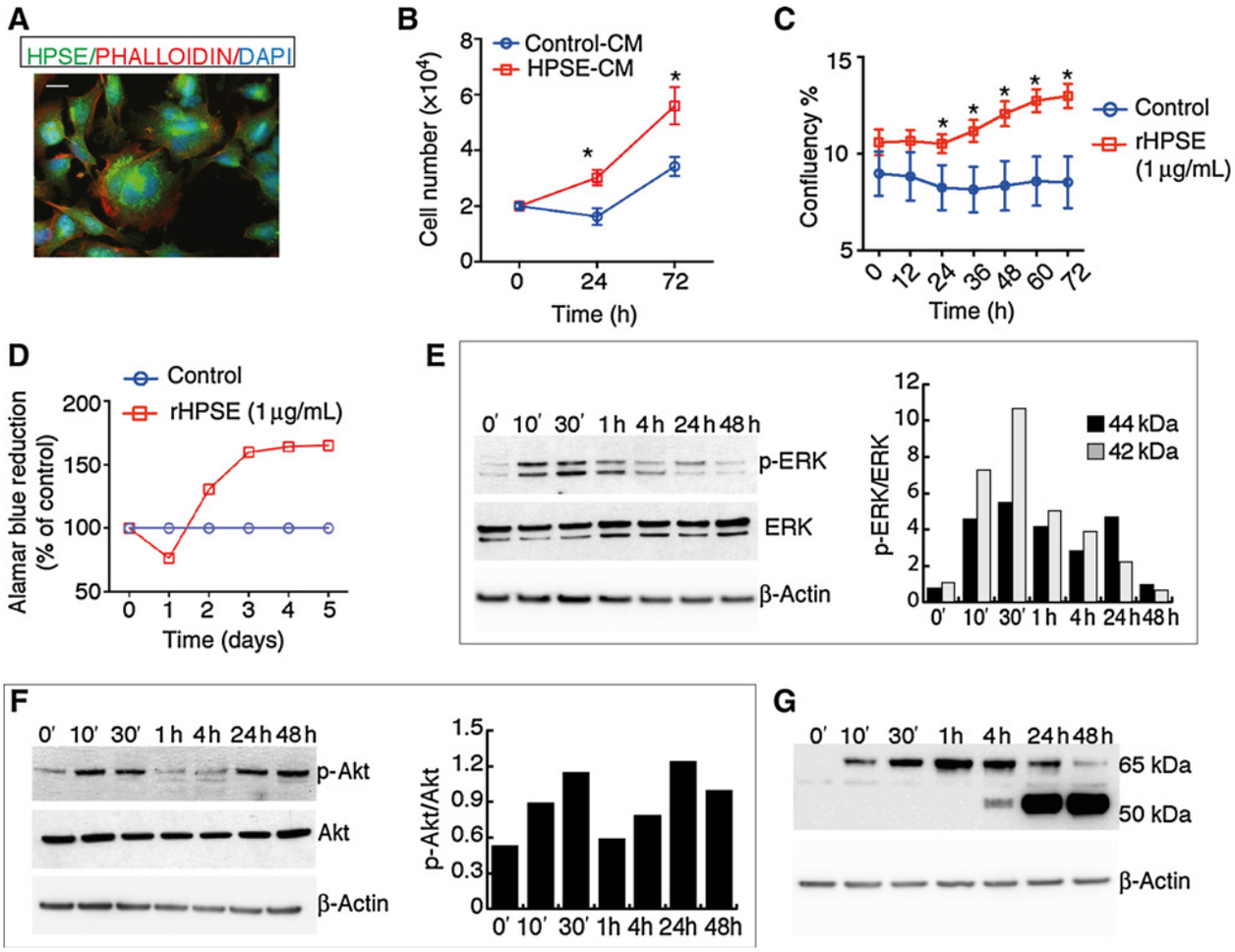

Figure 1.

HPSE confers a growth advantage on and enhances the viability of murine glioma cells while simultaneously activating their ERK and AKT pathways. **A,** Immunofluorescent staining of mouse glioma GL261 cells for HPSE (green) and F-actin with phalloidin (red) to delineate the cell structure. Scale bar, 20 μm. **B,** *In vitro* growth of GL261 cells in the presence of conditioned medium (CM) from CHO cells overexpressing HPSE (red line) or the corresponding control cells (blue line). Viable cells were counted for 72 hours after addition of the CM, and this experiment was repeated three times independently with 4 replicates each time ($n = 4$). The data were analyzed with the unpaired *t* test, *, $P < 0.05$. **C,** Growth curve of serum-starved (18 hours) GL261 cells for 72 hours in the presence or absence of recombinant HPSE (rHPSE, 1 μg/mL). Confluency (%) was determined with the IncuCyte imaging system once every 12 hours. The error bars indicate ± SD, and the data were analyzed utilizing the unpaired *t* test. ($n = 4$; *, $P < 0.05$). **D,** Alamar blue reduction (percentage of control) by GL261 cells incubated with rHPSE (1 μg/mL; red line) or vehicle alone (blue line). **E,** Activation of ERK in serum-starved GL261 cells by treatment with rHPSE (1 μg/mL), and cell lysates were collected and analyzed at the time-points indicated for pERK (top), total ERK (middle), and beta-actin (bottom). The bar graph illustrates the densitometric values for activated ERK (p44 and p42) normalized to the values of total ERK. **F,** AKT activation in GL261 cells, performed in a manner similar to **E**, With the bar graph depicting activated AKT normalized to total AKT. **G,** Internalization and processing of HPSE in GL261 cells for various periods of time after the addition of rHPSE lead to the levels of full-length (65-kDa) and processed 50-kDa forms indicated.

For *in vivo* imaging, 6 to 8 per group were anesthetized and injected intraperitoneally with luciferin (150 mg per kg body weight), and the intensity of the optical signal expressed as photon per second was captured using an IVIS CCD camera system (Xenogen). To quantify the luminescence, uniformly a specific region of interest (ROI) was defined and used in all the animals at all time points. For analysis, the Living Image 2.20 software (Xenogen) was used.

TMAs

TMA contained high-grade glioma (102 cases), low-grade glioma (80 cases), and nonmalignant control brain tissue ($n = 7$; ref. 26). HPSE antibody 733 (19) was used for immunohistochemistry. Staining procedures, scanning of slides, and image acquisition were performed as described (27). Human GBM tissue was obtained in accordance with an ethically reviewed and approved protocol (Uppsala 2007/353).

Database mining

Data on patient survival and tumor subtype were downloaded from The Cancer Genome Atlas (TCGA) Data Portal (http://tcga-data.nci.nih.gov). Expression values were obtained from the cBio Portal for Cancer Genomics (http://www.cbioportal.org).

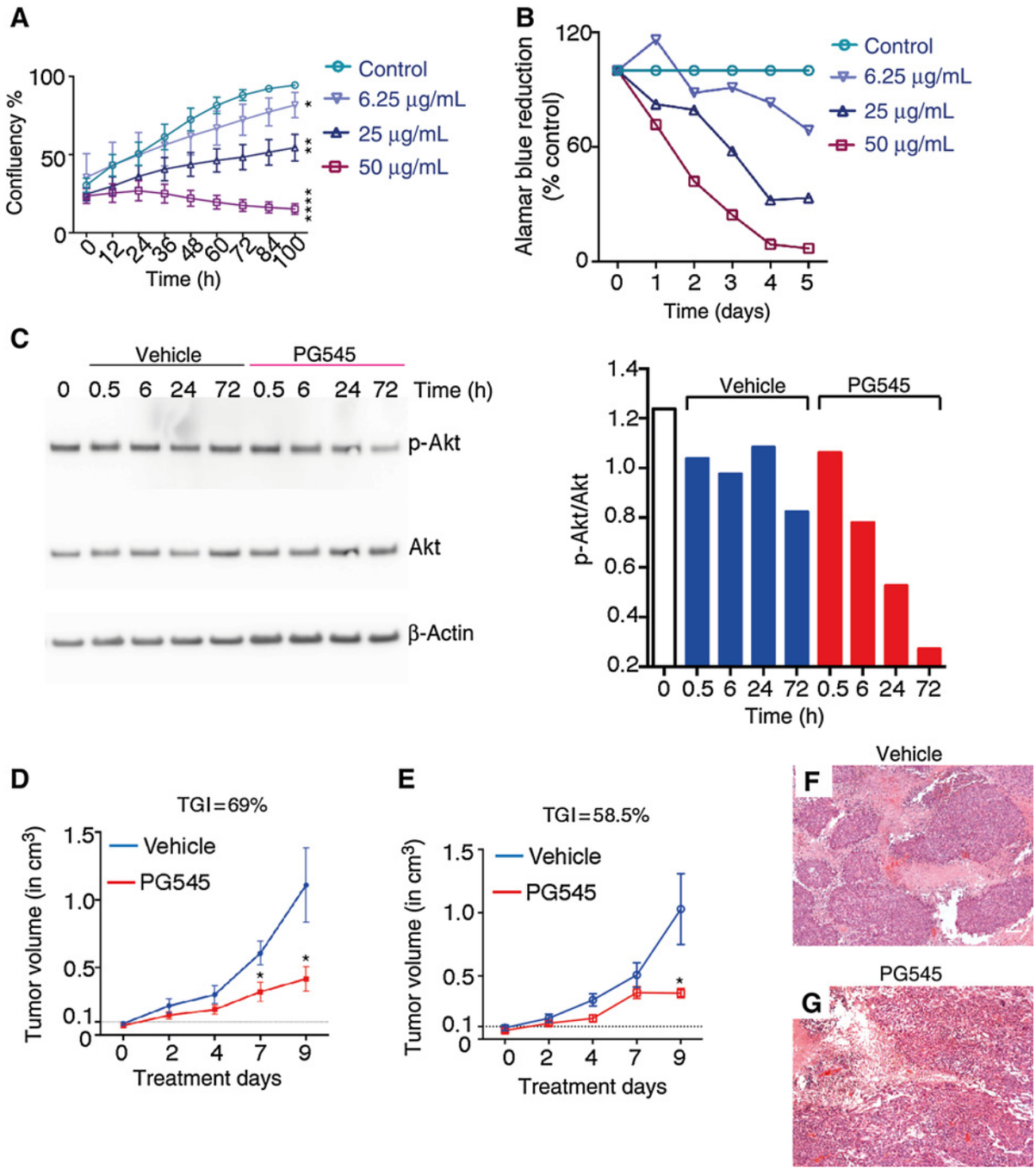

Figure 2.

Inhibition of HPSE reduces the proliferation, viability, and AKT activity of glioma cells *in vitro*, and reduces tumor burden *in vivo*. **A,** The growth of GL261 cells *in vitro* was monitored for 100 hours after addition of different concentrations of PG545, using the IncuCyte Imaging system ($n = 5$; *, $P < 0.05$; **, $P < 0.01$; ****, $P < 0.0001$). Analysis of the growth curves at different time-points and doses involved two-way ANOVA, followed by the multiple comparisons Dunnett test. The PG545- and vehicle-treated values were compared employing a two-tailed unpaired *t* test. **B,** Assessment of the viability of GL261 cells treated with a range of PG545 concentrations for specified periods of time. **C,** AKT activation in GL261 cells treated with PG545 (50 µg/mL) for 72 hours. The first four lanes represent cells treated with vehicle alone and the last four those treated with PG545. Top, pAKT; middle, total AKT; and bottom, beta-actin. Graphical representation of AKT activation normalized to the total amount of AKT. **D** and **E,** The volumes of subcutaneous GL261 tumors treated by intraperitoneal (**D**) or subcutaneous (next to the growing tumor) (**E**) injection of PG545 (red line) or vehicle alone (blue line; $n = 10$ mice/group; *, $P < 0.05$). TGI presented as a percentage of the growth of tumors treated with vehicle alone. Representative photographs of hematoxylin and eosin (H&E)-stained sections through subcutaneous tumors treated with (**F**) vehicle or (**G**) PG545. Scale bar, 100 µm.

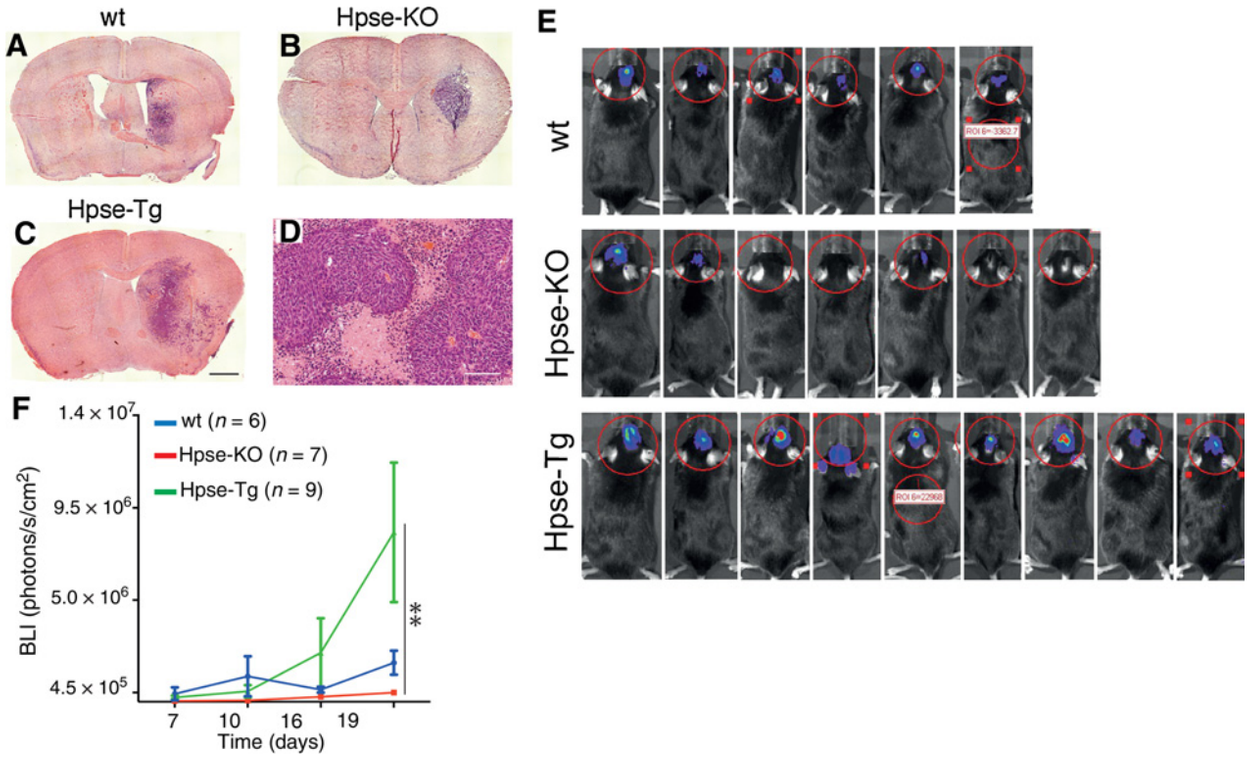

Figure 3.

The levels of HPSE in mouse brain determine the size of gliomas resulting from inoculated GL261 cells. **A–C,** Representative photographs of H&E-stained tumor-bearing coronal sections from the mouse brains of (**A**) wild-type (wt) (**B**) Hpse-KO and (**C**) Hpse-Tg mice. Scale bar = 1 mm. **D,** A representative microphotograph of H&E-stained section of a GL261-derived tumor in wt brain reveals infiltrative growth of the tumor cells. Scale bar = 100 mm. **E,** Photographs of the glioma-inoculated mice, analyzed for bioluminescence (BLI) by IVIS at day 19. **F,** A line graph of the average BLI signals obtained from the intracranial tumors at various time-points until day 19. The error bars represent means ± SD and the data were analyzed by two-way ANOVA, followed by Turkey's multiple comparisons test and reveal significant differences between the Hpse-Tg and Hpse-KO genotypes; **, $P < 0.01$; ***, $P < 0.001$.

Statistical analysis

All statistical analysis was performed using Prism version 5.0 or 6.0 (GraphPad Software, Inc.) or SPSS version 20 or 21 (IBM Corp.). Survival curves were plotted according to the Kaplan–Meier method, using the GraphPad Prism 5.0 Software.

Results

HPSE enhances the proliferation and viability, and stimulates ERK and AKT phosphorylation in murine glioma

To explore whether HPSE regulates glioma growth, we utilized GL261 cells (17) and found that expression of HPSE in these cells was robust with both cytoplasmic and nuclear staining (Fig. 1A). Conditioned medium from CHO cells engineered to overexpress HPSE (19) increased GL261 numbers (Fig. 1B), and treatment of these same cells with recombinant HPSE (rHPSE) not only elevated confluence (Fig. 1C), but also enhanced viability (Fig. 1D), thus showing a direct growth-stimulatory effect on glioma cells by HPSE.

ERK and AKT were rapidly phosphorylated in response to rHPSE (Fig. 1E and F), and to understand these effects, we monitored the internalization of rHPSE 65-kDa pro-enzyme and its proteolytic conversion to the enzymatically active form (50 kDa). The 50 kDa species appeared at 4 hours, and accumulated gradually until the 50 kDa form was predominant (Fig. 1G). We therefore conclude that the latent form of HPSE induced early activation of ERK and AKT by a nonenzymatic mechanism.

An inhibitor of HPSE reduced glioma growth and viability *in vitro* and *in vivo*

To determine whether inhibition of HPSE reduces tumor cell proliferation, we applied PG545, a potent inhibitor of the enzymatic activity of HPSE (28). PG545 reduced the growth of GL261 cells in a dose-dependent manner (Fig. 2A and Supplementary Fig. S1), and attenuated cell viability (Fig. 2B). In addition, PG545 lessened AKT activation (Fig. 2C) but not that of ERK (Supplementary Fig. S2).

Thereafter, we induced subcutaneous GL261 tumors in C57Bl/6J mice, and once tumor was palpable, we applied PG545 either intraperitoneally or subcutaneously. With intraperitoneal delivery, PG545 inhibited tumor growth by 69% (Fig. 2D), and the corresponding inhibition with subcutaneous administration was

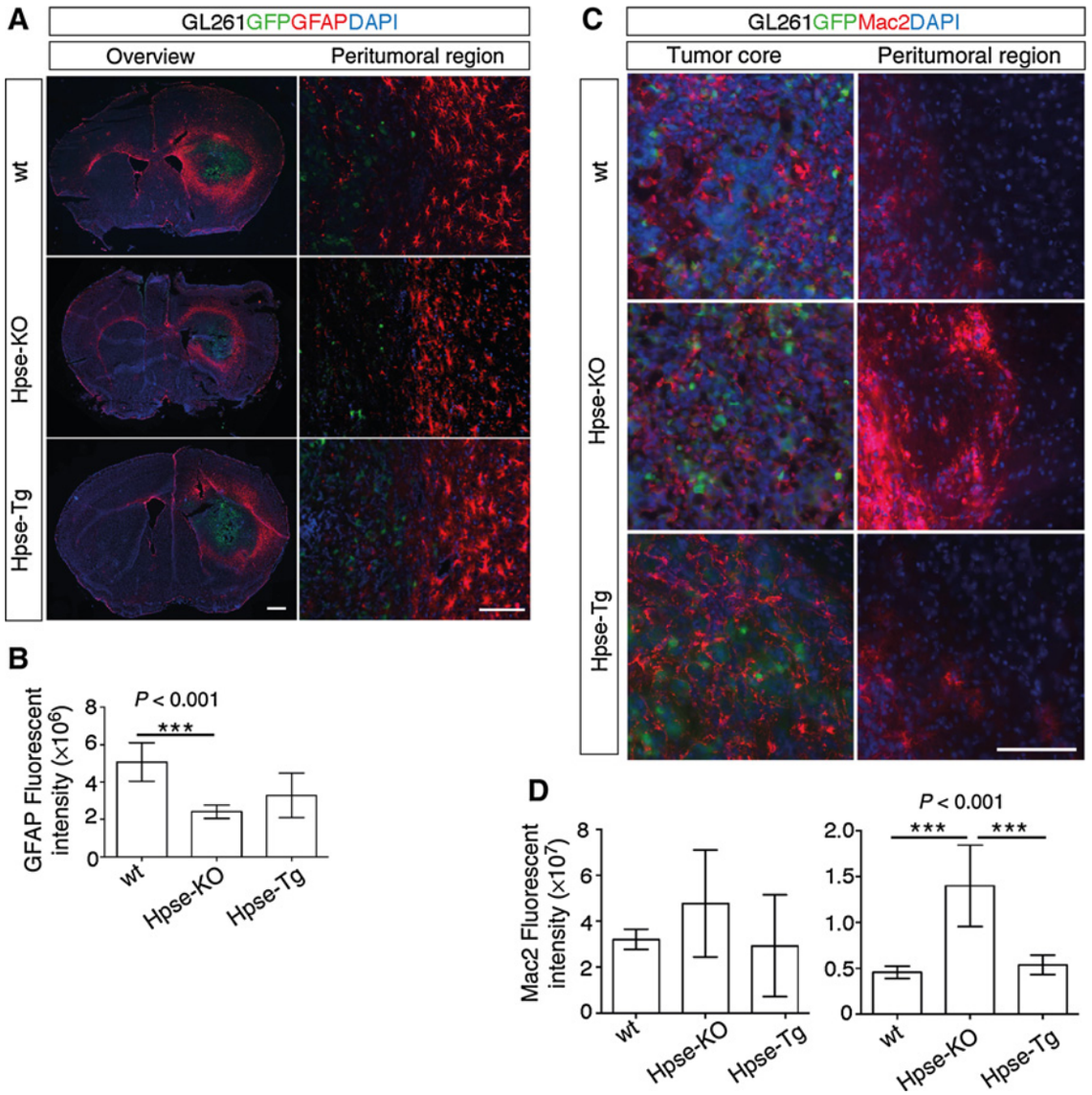

Figure 4.

The level of HPSE in the host mouse brain influences infiltration by astrocytes and microglia/macrophages. **A,** GFAP staining astrocytes (red) in coronal sections through the tumors in the brains of the different mouse strains showing an overview of the glial scar and the peritumoral region. The tumor cells expressing GFP appear in green. **B,** Quantitation of GFAP fluorescent staining in the peritumoral region. The data were analyzed using the unpaired *t* test (***, $P < 0.001$). **C,** Staining for Mac2 (red), a marker for microglia/macrophages, in the core and peritumoral region of brain tumors in animals of the three genotypes (tumor cells appear in green). **D,** The intensity of Mac2 staining in the tumor core (left) and peritumoral area (right; wt, $n = 3$; Hpse-KO, $n = 3$; Hpse-Tg, $n = 4$). These data were analyzed using the unpaired *t* test (***, $P < 0.001$). Scale bar, 100 μm.

58.5% (Fig. 2E). Histologic analysis of tumors treated with PG545 revealed a distinct morphology, with less nodular arrangement of tumor cells compared with the vehicle-treated tumors. (Fig. 2F and G and Supplementary Fig. S3).

HPSE levels in the host murine brain determine the tumorigenic potential of grafted murine glioma

Having established that HPSE influences the proliferation and survival of glioma cells and activates intracellular signaling pathways, we examined whether the level of HPSE in the host brain would affect tumor formation by injecting GL261 cells expressing luciferase into the striatum of HPSE transgenic mice (Hpse-Tg), HPSE knockout mice (Hpse-KO), and wild-type (wt) mice. Tumors formed in all three strains (Fig. 3A–C), and GL261 cells infiltrated the parenchyma (Fig. 3D). Bioluminescence monitoring revealed that the brain tumors in the Hpse-Tg animals grew faster than those in the Hpse-KO animals (Fig. 3E–F). We conclude that excessive degradation of HS by HPSE stimulated the growth and spread of glioma. On the other hand, the tumorigenic potential was hampered in the absence of host

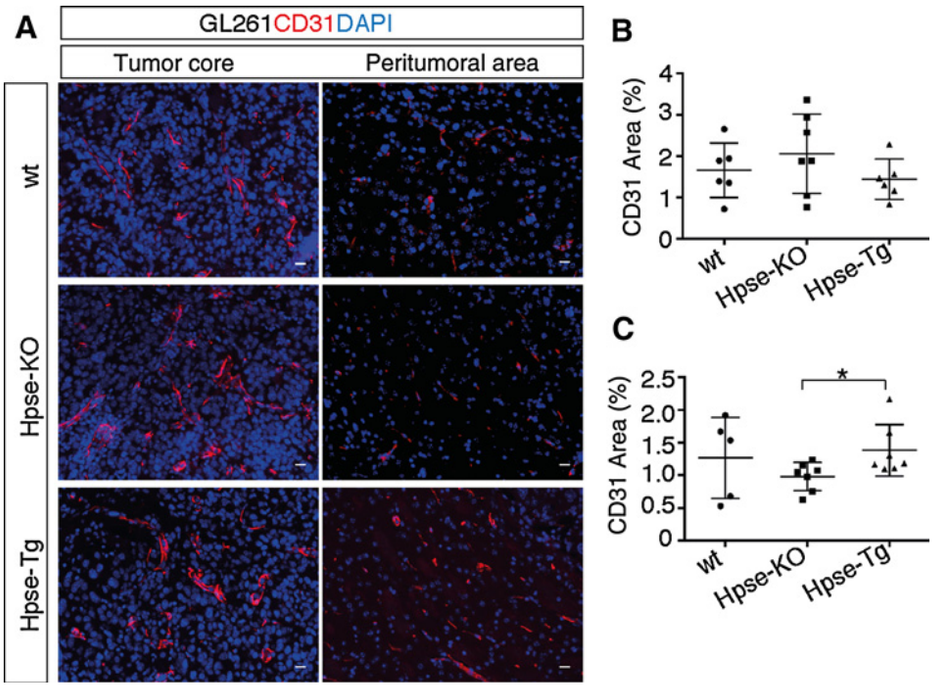

Figure 5.
HPSE influences peritumoral vessel density. **A,** Staining of the core and peritumoral region of tumors from all three genotypes for CD31 (red). Graphical representation of the CD31 staining in **A** (percentage) in the tumor core (**B**) and peritumoral region (**C**) was quantified using ImageJ (5 mice per genotype); *, $P < 0.05$. Scale bar, 10 μm.

brain–derived HPSE, but since the GL261 tumor cells expressed HPSE, the enzyme was not entirely lacking.

The level of HPSE influences the tumor microenvironment

Tumor-associated astrocytes have been implicated in glioma progression, and we therefore stained for GFAP-positive astrocytes (Fig. 4A). The glial scar surrounding the tumors in the Hpse-KO brain was thinner than in the wt brain (Fig. 4B), indicating that the absence of HPSE from the micro milieu lowered the reactivity of host brain astrocytes. Microglia/macrophages, the most abundant tumor-associated cells, were visualized with antibodies to Mac2 (Fig. 4C). The peritumoral region of the Hpse-KO brain was more extensively stained (Fig. 4D, right), suggesting that HPSE levels influence the attraction of microglia/macrophages to the tumor. The tumor cores were equally densely packed with Mac2-positive cells (Fig. 4D, left).

Tumors were next stained with anti-CD31 antibodies to monitor vascularization (Fig. 5A). Hpse-Tg tumors displayed more CD31 staining in the peritumoral area than Hpse-KO brains (Fig. 5C), while in the tumor core, no difference was detected (Fig. 5B). Costaining for desmin, a pericyte marker, did not differ (Supplementary Fig. S4). These findings constitute evidence that the density of tumor microvasculature, but not their pericyte coverage, was influenced by HPSE.

HPSE is expressed by human GBM cells and confers a growth advantage

We recently established clinically annotated and experimentally validated cell lines from GBM patients (18). HPSE staining revealed high expression (Fig. 6A), and Western blotting showed higher level of expression of both the 65-kDa and the 50-kDa forms in these GBM cells compared with control brain (Fig. 6B). Decreasing HPSE in U3013MG (Fig. 6C) reduced cell numbers (Fig. 6D), and PG545 reduced GBM cell confluency (Fig. 6E) further demonstrating that GBM cell proliferation can be attenuated by lowering the level of HPSE.

Forty-eight of our GBM lines, assigned to subclasses (18), were analyzed for HPSE mRNA expression (Fig. 6F). Mesenchymal GBM cells expressed HPSE at the highest level, with the most pronounced difference being in comparison with the Classical and Neural subtypes. Similarly, when analyzing the TCGA dataset, expression of HPSE was highest in the Mesenchymal subtype (Fig. 6G), suggesting that HPSE expression reflects GBM heterogeneity.

HPSE is upregulated in human glioma, with more pronounced staining of the neuropil in high-grade tumors

HPSE staining of brain tumor TMAs revealed low levels of HPSE in normal tissue and elevated levels in glioma of all grades (Fig. 7A). In addition to cytoplasmic HPSE, we detected HPSE in the nucleus (29). Diffuse HPSE immunoreactivity was also observed in the intercellular space of tumor cores, indicative of secretion. Neuropathological annotation assessed intensity and fraction of stained cells. Although the neuropil of all high-grade glioma stained either moderately or strongly for HPSE, 8% of the low-grade tumors were stained negatively or weakly, and there were fewer cases of strong staining in this latter group (Fig. 7B). Thus, the neuropil of high-grade glioma contain higher levels of HPSE than those of low-grade tumors.

Nuclear expression of HPSE in high-grade glioma is associated with shorter survival of patients

The 3-year overall survival was significantly greater in cases in which the tumor cells exhibited <75% nuclear staining for HPSE (Fig. 7C) with a median survival of 403 ± 34 days compared with 279 ± 28 days for those with ≥75% nuclear staining of their tumor cell nuclei. Next, we compared expression data from the

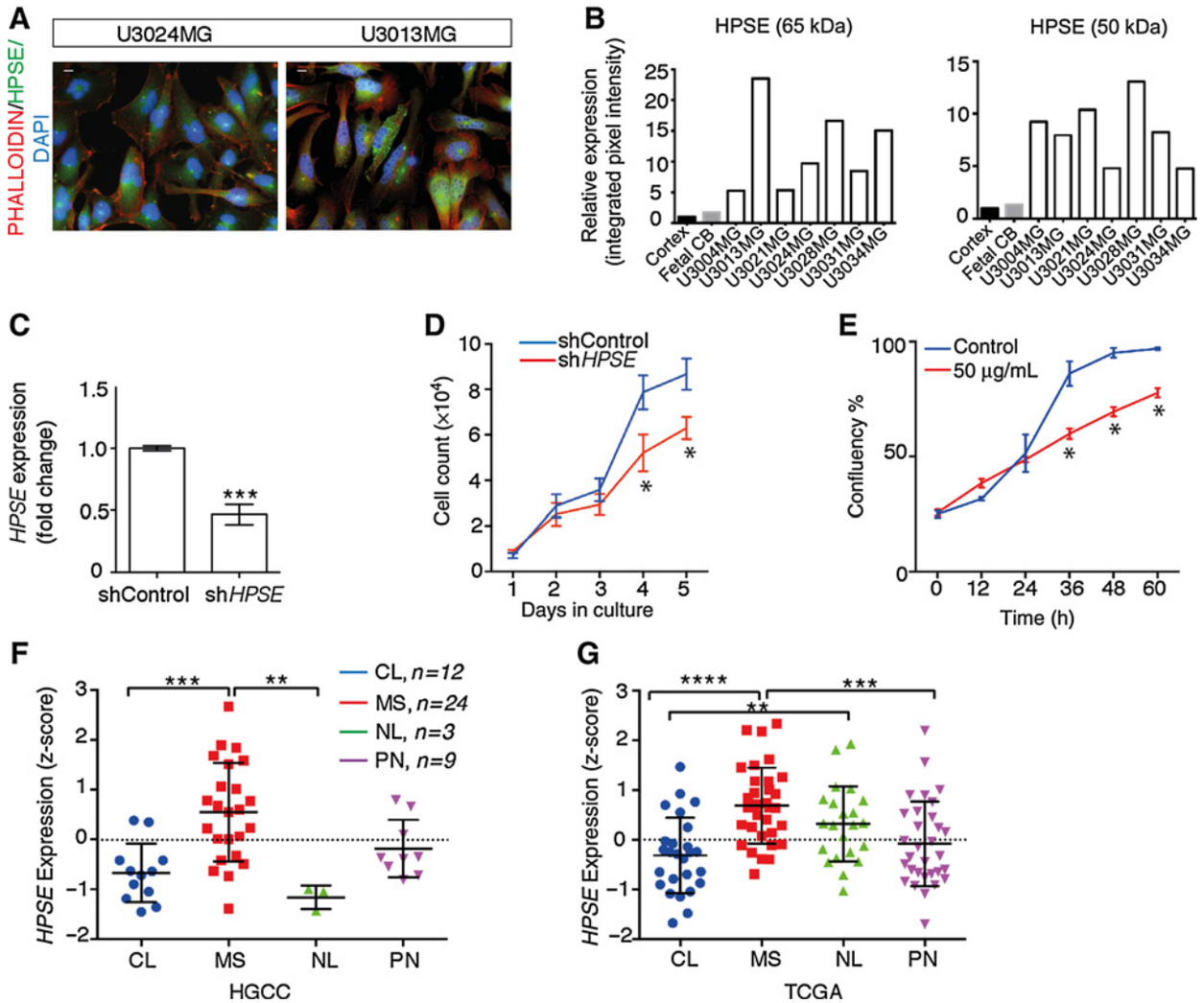

Figure 6.

HPSE is expressed by human GBM cell lines, and its silencing reduces the rate of cell growth. **A,** Immunofluorescent staining of the human U3024MG and U3013MG GBM cell lines for HPSE (green) and staining of F-actin with phalloidin (red). Scale bars, 10 µm. **B,** Quantification of Western blots of the 65 kDa and 50 kDa form in 7 GBM cell lines and normal brain (adult frontal cortex and fetal cerebellum). These values have been normalized to the level of beta actin. **C,** Quantitative PCR shows reduced HPSE mRNA after shHPSE lentiviral targeting of U3013MG cells. **D,** Growth of U3013MG cells transduced with either shHPSE or scrambled shControl cultured for 5 days in defined medium supplemented with FGF2 and EGF (*, $P = 0.001$; $n = 4$). **E,** Growth of U3013MG cells after addition of PG545, using the IncuCyte Imaging system (*, $P < 0.05$). Analysis of the growth curves involved two-way ANOVA, followed by the multiple comparison's Dunnett test. The PG545- and vehicle-treated values were compared employing a two-tailed unpaired *t* test (**F**) *HPSE* expression, in terms of Z-score, in 48 human GBM cell lines assigned to molecular subtypes on the basis of their genetic signatures (mesenchymal, $n = 24$; classical, $n = 12$; proneural, $n = 9$; neural, $n = 3$). Analysis of the data by one-way ANOVA and Turkey multiple comparison revealed significant differences in gene expression (*, $P < 0.05$). **G,** Comparison of the normalized expression (Z-scores) of HPSE in the TCGA database across subtypes (mesenchymal, $n = 30$; neural, $n = 18$; proneural, $n = 29$; classical, $n = 25$). Error bars denote ± SD. A negative Z-score indicates a level of expression below the mean for that subtype with the difference being expressed as units of SD. These data were analyzed by one-way ANOVA ($P < 0.0001$) and Turkey multiple comparison revealed significant differences in gene expression (*, $P < 0.05$; **, $P < 0.01$; ***, $P < 0.001$; and ****, $P < 0.0001$).

cBio Cancer Genomics Portal (30) with GBM patient survival (31). A Kaplan–Meier survival plot for the 30% of patients with lowest HPSE expression and the 30% with highest showed longer survival for the former (Fig. 7D). Based on data from our own cohort, and that of TCGA/cBio Portal, we conclude that high expression of HPSE in high-grade glioma is associated with a worse outcome.

Discussion

Here, we demonstrate that HPSE, the HS-cleaving enzyme, exerts major impacts on the growth and progression of malignant glioma. We document effects *in vitro* and *in vivo* that can be ascribed to both enzymatic and nonenzymatic properties of HPSE. Our experiments downregulating HPSE, and using the

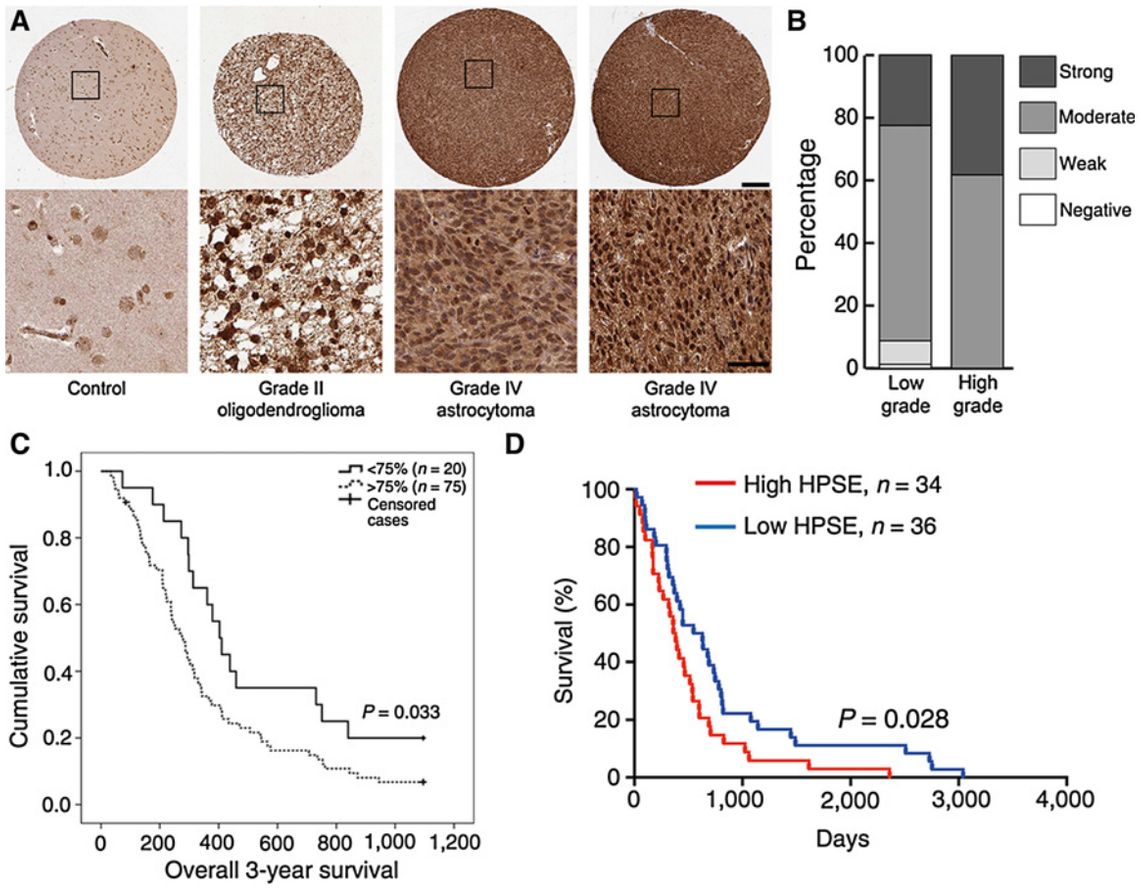

Figure 7.

Heparanase is upregulated in human glioma, with more pronounced neuropil staining in high-grade tumors. **A,** Representative staining of glioma tissue with an anti-HPSE antibody (Ab733): from left to right, control (nontumor human brain), low-grade glioma, and two high-grade gliomas. Scale bar, 200 μm (overview, top), 50 μm (inset, bottom). Cytoplasmic staining, nuclear, and neuropil staining for HPSE designated as negative, weak, moderate, or strong and the fraction of stained cells/neuropil as 0%–1%, 2%–10%, 11%–25%, 26%–50%, 50%–75%, or >75%. **B,** Stacked bar chart depicting the percentages of cases with negative, weak, moderate, and strong staining intensity for HPSE in the neuropil of high-grade and low-grade glioma. There was a significant negative correlation between the staining intensity of the neuropil and low-grade tumors (Spearman, −0.218, $P = 0.003$). **C,** Kaplan–Meier curve for overall survival (3 years) of patients with high-grade glioma, categorized as exhibiting <75% (solid line $n = 20$) and >75% (dotted line $n = 75$) nuclear staining of their cancer cells ($P = 0.033$). Survival for the latter group was 403 days ± 34, compared with 279 days ± 28. **D,** When a group of patients with GBM was analyzed with respect to survival (the TCGA database) and expression data for HPSE (from the cBio portal), a Kaplan–Meier survival curve showed shorter survival of patients with high expression of *HPSE* ($n = 34$, $HPSE_{high}$) than those exhibiting low expression ($n = 29$ $HPSE_{low}$) $P = 0.03$. The Log-rank (Mantel–Cox) test was applied for analysis of the survival curve.

HS mimetics PG545, previously shown to exert antimetastatic (32) and antiangiogenic (33) effects against other solid tumors, demonstrated that growth of glioma cells can be attenuated by inhibition of HPSE activity. This is the first demonstration that blocking HS fragmentation and other HPSE-associated protumorigenic effects reduced the growth of brain tumors. In addition to HPSE inhibition, PG545 has been ascribed antitumor activity, e.g., through blocking of WNT signaling (34). Therefore, its inhibitory effects on glioma may be explained partly by targeting other parameters than the enzymatic activity of HPSE. Indeed, we find effects on glioma cells that must be enzyme-independent since ERK and AKT became phosphorylated well before the latent HPSE was converted into its 50-kDa enzymatically active form. Nonenzymatic activation of AKT by HPSE has been proposed (35), mediated by FAK or PYK2 (36), but the underlying mechanism remains unknown. However, our present observations clearly support additional protumorigenic effects of HPSE that are independent of its enzymatic activity.

Undoubtedly, HPSE exerts pro-tumorigenic effects on glioma since the brain tumors in mice with elevated levels of HPSE grew to a larger size, while those in mice lacking the HPSE gene were much smaller. In addition to stimulating the tumor cells themselves, HPSE could enhance tumor growth through modulation of the glioma microenvironment through multiple mechanisms. The ability of reactive astrocytes to relocate to the tumor microenvironment depends on HPSE levels because the glial scar was thinner in Hpse-KO mice. This indicates a difference to CS-GAG–enriched matrices that have been reported to repel astrocytes (37). A distinct interface

between tumor cells and astrocytes was seen regardless of whether the HS chains are highly fragmented, as in the Hpse-Tg brain, or more intact, as in the Hpse-KO mice (24, 25) leading us to propose that CS-GAGs and HS-GAGs play different roles in the tumor microenvironment.

Microglia/macrophages, the predominant cell type associated with glioma, are generally reported to be protumorigenic (5) but also elicit an antitumor immune response (38, 39), and there is believed to be a continuum between their phenotypes. We found, somewhat surprisingly, that the peritumoral region in the Hpse-KO mouse brain harbored more Mac2-positive cells than the wt or Hpse-Tg brain. HPSE-Tg brains have shown attenuated microglial activation (40). Thus, in the glioma microenvironment in Hpse-KO mice, lack of HPSE may have shifted the phenotype of resident microglia and recruited macrophages toward an antitumor direction.

The increase in peritumoral CD31 staining in Hpse-Tg brains could be attributed to an elevated bioavailability of endothelial mitogens released upon HS degradation. Conversely, the longer and homogeneous HS chains (25) in Hpse-KO mice might limit the availability of proangiogenic factors. Pericyte coverage was similar among the three mouse strains, suggesting that HPSE does not affect vascular permeability.

Our recent collection of annotated cell lines derived from GBM patients covers much of the GBM heterogeneity (18), and HPSE levels in all cell lines examined were above those in normal brain. This is in line with our patient cohorts and confirms upregulated HPSE in glioma. Although the intensity and localization of HPSE staining varied between the patients in our cohorts, nontumorous brain tissue was always weakly stained. Previously, Ueno and colleagues (41) reported that HPSE mRNA was virtually undetectable and HPSE immunoreactivity absent from human GBMs. Our present observations are more in line with those of Hong and colleagues (42), who describe enhanced levels of HPSE mRNA in glioma, but no correlation to the degree of malignancy, possibly due to their limited number of patients (42). Based on our mouse data that differing HPSE amounts in the tumor microenvironment affects tumor size, we propose that surface-associated or secreted HPSE supports the highly invasive properties of high-grade gliomas and, consequently, enhance tumor progression. This is supported by our observation that among our 182 patients, we found that low-grade gliomas were less intensely stained by anti-HPSE antibodies in the neuropil than high-grade gliomas.

Both in the TCGA cohort (2) and our patient-derived cell lines, the mesenchymal subtype exhibited highest HPSE expression. This subtype is characterized by NF1 deletion, together with elevated expression of genes encoding members of the TNFa superfamily and components of the NF-kB pathway genes. Interestingly, Wade and colleagues (8) have reported that Syndecan-1 (SDC1), a proteoglycan core protein which is dependent on NF-κB activation in glioma (43) and interacts with HPSE to enhance tumor growth (44), is highly expressed in mesenchymal GBM. We therefore speculate that interrupting the HPSE-SDC1 axis would prove beneficial when treating mesenchymal GBM.

To our knowledge, this is the first report linking elevated levels of HPSE to reduced survival of patients with brain tumors, and our findings thus suggest that HPSE may be of clinical importance. Increased HPSE expression has been previously associated with reduced postoperative survival in other solid tumors, e.g., colorectal (45), pancreatic (46), and lung cancer (47). Our finding that it was the nuclear fraction of HPSE that correlated to glioma grade may seem unexpected. However, it has long been known that HSPGs can localize to the nucleus of both normal and neoplastic cells, and although modulation of cellular distribution of growth factors may provide one explanation for this, the process is not yet fully understood (48).

In summary, our observations reveal that HPSE confers a growth advantage on glioma cells, both *in vitro* and *in vivo*, and thus suggests that it could be clinically relevant to target HPSE in glioma.

Disclosure of Potential Conflicts of Interest

No potential conflicts of interest were disclosed.

Authors' Contributions

Conception and design: S. Kundu, A. Xiong, A. Spyrou, G. Wicher, I. Vlodavsky, J.-P. Li, K. Forsberg-Nilsson

Development of methodology: S. Kundu, A. Xiong, A. Spyrou, L. Zhang

Acquisition of data (provided animals, acquired and managed patients, provided facilities, etc.): S. Kundu, A. Xiong, G. Wicher, P.-H.D. Edqvist, A. Dimberg, A. Smits, I. Vlodavsky, J.-P. Li

Analysis and interpretation of data (e.g., statistical analysis, biostatistics, computational analysis): S. Kundu, A. Xiong, G. Wicher, P.-H.D. Edqvist, N. Ilan, K. Forsberg-Nilsson

Writing, review, and/or revision of the manuscript: S. Kundu, A. Xiong, A. Spyrou, G. Wicher, A. Dimberg, A. Smits, I. Vlodavsky, J.-P. Li, K. Forsberg-Nilsson

Administrative, technical, or material support (i.e., reporting or organizing data, constructing databases): S. Kundu, M. Essand, N. Ilan, K. Forsberg-Nilsson

Study supervision: S. Kundu, J.-P. Li, K. Forsberg-Nilsson

Acknowledgments

We wish to thank A. Hermansson and A.-C. Hellström for excellent technical assistance, and the personnel at the Rudbeck and BMC Animal Facility for animal care. We thank Dr. S. Kundu, Uppsala University, for help with analysis of Incucyte data. Drs. K. Dredge and E. Hammond, Progen Biochemicals, are acknowledged for generously providing PG545. We acknowledge the assistance and support of the SciLifeLab BioVis Facility Uppsala, Sweden.

Grant Support

This study was supported by grants from the Swedish Cancer Society (130500 to K. Forsberg-Nilsson), Swedish Research Council (521-2013-3356 to K. Forsberg-Nilsson), Swedish Childhood Cancer Foundation (PROJ12/093 to K. Forsberg-Nilsson), and Linnaeus Foundation (2012 to S. Kundu).

The costs of publication of this article were defrayed in part by the payment of page charges. This article must therefore be hereby marked *advertisement* in accordance with 18 U.S.C. Section 1734 solely to indicate this fact.

Received July 28, 2016; revised August 8, 2016; accepted August 12, 2016; published OnlineFirst August 26, 2016.

References

1. Stupp R, Mason WP, van den Bent MJ, Weller M, Fisher B, Taphoorn MJ, et al. Radiotherapy plus concomitant and adjuvant temozolomide for glioblastoma. N Engl J Med 2005;352:987–96.
2. Verhaak RG, Hoadley KA, Purdom E, Wang V, Qi Y, Wilkerson MD, et al. Integrated genomic analysis identifies clinically relevant subtypes of glioblastoma characterized by abnormalities in PDGFRA, IDH1, EGFR, and NF1. Cancer Cell 2010;17:98–110.
3. Goldshmidt O, Nadav L, Aingorn H, Irit C, Feinstein N, Ilan N, et al. Human heparanase is localized within lysosomes in a stable form. Exp Cell Res 2002;281:50–62.

4. Nakada M, Nakada S, Demuth T, Tran NL, Hoelzinger DB, Berens ME. Molecular targets of glioma invasion. Cell Mol Life Sci 2007;64: 458–78.
5. Charles NA, Holland EC, Gilbertson R, Glass R, Kettenmann H. The brain tumor microenvironment. Glia 2011;59:1169–80.
6. Bellail AC, Hunter SB, Brat DJ, Tan C, Van Meir EG. Microregional extracellular matrix heterogeneity in brain modulates glioma cell invasion. Int J Biochem Cell Biol 2004;36:1046–69.
7. Xiong A, Kundu S, Forsberg-Nilsson K. Heparan sulfate in the regulation of neural differentiation and glioma development. FEBS J 2014;281:4993–5008.
8. Wade A, Robinson AE, Engler JR, Petritsch C, James CD, Phillips JJ. Proteoglycans and their roles in brain cancer. FEBS J 2013;280:2399–417.
9. Esko JD, Lindahl U. Molecular diversity of heparan sulfate. J Clin Invest 2001;108:169–73.
10. Habuchi H, Habuchi O, Kimata K. Sulfation pattern in glycosaminoglycan: Does it have a code? Glycoconj J 2004;21:47–52.
11. Vlodavsky I, Beckhove P, Lerner I, Pisano C, Meirovitz A, Ilan N, et al. Significance of heparanase in cancer and inflammation. Cancer Microenviron 2012;5:115–32.
12. Hulett MD, Freeman C, Hamdorf BJ, Baker RT, Harris MJ, Parish CR. Cloning of mammalian heparanase, an important enzyme in tumor invasion and metastasis. Nat Med 1999;5:803–9.
13. Vlodavsky I, Friedmann Y, Elkin M, Aingorn H, Atzmon R, Ishai-Michaeli R, et al. Mammalian heparanase: Gene cloning, expression and function in tumor progression and metastasis. Nat Med 1999;5:793–802.
14. Koliopanos A, Friess H, Kleeff J, Shi X, Liao Q, Pecker I, et al. Heparanase expression in primary and metastatic pancreatic cancer. Cancer Res 2001; 61:4655–9.
15. Ben-Izhak O, Kaplan-Cohen V, Ilan N, Gan S, Vlodavsky I, Nagler R. Heparanase expression in malignant salivary gland tumors inversely correlates with long-term survival. Neoplasia 2006;8:879–84.
16. Ilan N, Elkin M, Vlodavsky I. Regulation, function and clinical significance of heparanase in cancer metastasis and angiogenesis. Int J Biochem Cell Biol 2006;38:2018–39.
17. Szatmari T, Lumniczky K, Desaknai S, Trajcevski S, Hidvegi EJ, Hamada H, et al. Detailed characterization of the mouse glioma 261 tumor model for experimental glioblastoma therapy. Cancer Sci 2006;97: 546–53.
18. Xie Y, Bergstrom T, Jiang Y, Johansson P, Marinescu VD, Lindberg N, et al. The human glioblastoma cell culture resource: Validated cell models representing all molecular subtypes. EBioMedicine 2015;2:1351–63.
19. Zetser A, Levy-Adam F, Kaplan V, Gingis-Velitski S, Bashenko Y, Schubert S, et al. Processing and activation of latent heparanase occurs in lysosomes. J Cell Sci 2004;117(Pt 11):2249–58.
20. Bergstrom T, Holmqvist K, Tararuk T, Johansson S, Forsberg-Nilsson K. Developmentally regulated collagen/integrin interactions confer adhesive properties to early postnatal neural stem cells. Biochim Biophys Acta 2014; 1840:2526–32.
21. Zhang L, Kundu S, Feenstra T, Li X, Jin C, Laaniste L, et al. Pleiotrophin promotes vascular abnormalization in gliomas and correlates with poor survival in patients with astrocytomas. Sci Signal 2015;8:ra125.
22. Purushothaman A, Chen L, Yang Y, Sanderson RD. Heparanase stimulation of protease expression implicates it as a master regulator of the aggressive tumor phenotype in myeloma. J Biol Chem 2008;283: 32628–36.
23. Jin C, Yu D, Hillerdal V, Wallgren A, Karlsson-Parra A, Essand M. Allogeneic lymphocyte-licensed DCs expand T cells with improved antitumor activity and resistance to oxidative stress and immunosuppressive factors. Mol Ther Methods Clin Dev 2014;1:14001.
24. Zcharia E, Metzger S, Chajek-Shaul T, Aingorn H, Elkin M, Friedmann Y, et al. Transgenic expression of mammalian heparanase uncovers physiological functions of heparan sulfate in tissue morphogenesis, vascularization, and feeding behavior. FASEB J 2004;18:252–63.
25. Zcharia E, Jia J, Zhang X, Baraz L, Lindahl U, Peretz T, et al. Newly generated heparanase knock-out mice unravel co-regulation of heparanase and matrix metalloproteinases. PLoS One 2009;4:e5181.
26. Polajeva J, Bergstrom T, Edqvist PH, Lundequist A, Sjosten A, Nilsson G, et al. Glioma-derived macrophage migration inhibitory factor (MIF) promotes mast cell recruitment in a STAT5-dependent manner. Mol Oncol 2014;8:50–8.
27. Kampf C, Olsson I, Ryberg U, Sjostedt E, Ponten F. Production of tissue microarrays, immunohistochemistry staining and digitalization within the human protein atlas. J Vis Exp 2012.
28. Hammond E, Handley P, Dredge K, Bytheway I. Mechanisms of heparanase inhibition by the heparan sulfate mimetic PG545 and three structural analogues. FEBS Open Bio 2013;3:346–51.
29. Schubert SY, Ilan N, Shushy M, Ben-Izhak O, Vlodavsky I, Goldshmidt O. Human heparanase nuclear localization and enzymatic activity. Lab Invest 2004;84:535–44.
30. Cerami E, Gao J, Dogrusoz U, Gross BE, Sumer SO, Aksoy BA, et al. The cBio cancer genomics portal: An open platform for exploring multidimensional cancer genomics data. Cancer Discov 2012;2:401–4.
31. Network. CGAR. Comprehensive genomic characterization defines human glioblastoma genes and core pathways. Nature 2008;455:1061–8.
32. Dredge K, Hammond E, Handley P, Gonda TJ, Smith MT, Vincent C, et al. PG545, a dual heparanase and angiogenesis inhibitor, induces potent anti-tumour and anti-metastatic efficacy in preclinical models. Br J Cancer 2011;104:635–42.
33. Ferro V, Liu L, Johnstone KD, Wimmer N, Karoli T, Handley P, et al. Discovery of PG545: A highly potent and simultaneous inhibitor of angiogenesis, tumor growth, and metastasis. J Med Chem 2012;55: 3804–13.
34. Jung DB, Yun M, Kim EO, Kim J, Kim B, Jung JH, et al. The heparan sulfate mimetic PG545 interferes with Wnt/beta-catenin signaling and significantly suppresses pancreatic tumorigenesis alone and in combination with gemcitabine. Oncotarget 2015;6:4992–5004.
35. Ben-Zaken O, Gingis-Velitski S, Vlodavsky I, Ilan N. Heparanase induces Akt phosphorylation via a lipid raft receptor. Biochem Biophys Res Commun 2007;361:829–34.
36. Riaz A, Ilan N, Vlodavsky I, Li JP, Johansson S. Characterization of heparanase-induced phosphatidylinositol 3-kinase-AKT activation and its integrin dependence. J Biol Chem 2013;288:12366–75.
37. Silver DJ, Siebzehnrubl FA, Schildts MJ, Yachnis AT, Smith GM, Smith AA, et al. Chondroitin sulfate proteoglycans potently inhibit invasion and serve as a central organizer of the brain tumor microenvironment. J Neurosci 2013;33:15603–17.
38. Villeneuve J, Tremblay P, Vallieres L. Tumor necrosis factor reduces brain tumor growth by enhancing macrophage recruitment and microcyst formation. Cancer Res 2005;65:3928–36.
39. Sarkar S, Doring A, Zemp FJ, Silva C, Lun X, Wang X, et al. Therapeutic activation of macrophages and microglia to suppress brain tumor-initiating cells. Nat Neurosci 2014;17:46–55.
40. O'Callaghan P, Li JP, Lannfelt L, Lindahl U, Zhang X. Microglial heparan sulfate proteoglycans facilitate the cluster-of-differentiation 14 (CD14)/toll-like receptor 4 (TLR4)-dependent inflammatory response. J Biol Chem 2015;290:14904–14.
41. Ueno Y, Yamamoto M, Vlodavsky I, Pecker I, Ohshima K, Fukushima T. Decreased expression of heparanase in glioblastoma multiforme. J Neurosurg 2005;102:513–21.
42. Hong X, Nelson KK, deCarvalho AC, Kalkanis SN. Heparanase expression of glioma in human and animal models. J Neurosurg 2010;113:261–9.
43. Watanabe A, Mabuchi T, Satoh E, Furuya K, Zhang L, Maeda S, et al. Expression of syndecans, a heparan sulfate proteoglycan, in malignant gliomas: Participation of nuclear factor-kappaB in upregulation of syndecan-1 expression. J Neurooncol 2006;77:25–32.
44. Ramani VC, Purushothaman A, Stewart MD, Thompson CA, Vlodavsky I, Au JL, et al. The heparanase/syndecan-1 axis in cancer: Mechanisms and therapies. FEBS J 2013;280:2294–306.
45. Sato T, Yamaguchi A, Goi T, Hirono Y, Takeuchi K, Katayama K, et al. Heparanase expression in human colorectal cancer and its relationship to tumor angiogenesis, hematogenous metastasis, and prognosis. J Surg Oncol 2004;87:174–81.
46. Kim AW, Xu X, Hollinger EF, Gattuso P, Godellas CV, Prinz RA. Human heparanase-1 gene expression in pancreatic adenocarcinoma. J Gastrointest Surg 2002;6:167–72.
47. Cohen E, Doweck I, Naroditsky I, Ben-Izhak O, Kremer R, Best LA, et al. Heparanase is overexpressed in lung cancer and correlates inversely with patient survival. Cancer 2008;113:1004–11.
48. Fedarko NS, Conrad HE. A unique heparan sulfate in the nuclei of hepatocytes: Structural changes with the growth state of the cells. J Cell Biol 1986;102:587–99.